Stability and Quantization Error Analysis of Haptic Rendering of Virtual Stiffness and Damping

Nick Colonnese and Allison Okamura

Abstract

Stable, quantization error noise free, rendering of high-stiffness dynamics can be challenging using impedance-type haptic displays. In this paper, we examine a canonical one degree-of-freedom haptic display rendering a virtual spring and damper including the effects of device and human dynamics, sampling, position quantization, time delay, and the low-pass filter operating on the device velocity estimate. We construct various stability and quantization error regions as a function of system parameters, showing the necessary trade-offs that occur between them. Although we apply the quantization error analysis to virtual spring and damper rendering, it applies to a *general* virtual environment: we present sufficiency for quantization error passivity, necessity for no malicious touch limit cycles, and necessity for no uncoupled touch limit cycles. Using these results, aided by supplementary code we present, we find control parameters to render the largest renderable virtual stiffness for a given haptic display. The analytical results are experimentally verified using a Phantom Premium 1.5 haptic device.

Index Terms

L.2.0.a [Haptics]: Kinesthetic devices; L.2.0.u [Haptics] System design and analysis; L.2.0.o [Haptics]: Transparency.

I. Introduction

FOR many applications of kinesthetic (force feedback) haptic displays, we aim to render the stiffest possible dynamics to the human user. Rendering stiff dynamics can be accomplished through *virtual spring and damper rendering*, where the actuators of the haptic device produce forces proportional to position and velocity. Display of stiffness and damping is used for most haptic display applications, and serves as a fundamental building block for rendering more complicated virtual environments. However,

Nick Colonnese and Allison Okamura are with the Mechanical Engineering Department, Stanford University, Stanford, CA, 94305. E-mail: ncolonnese@stanford.edu, aokamura@stanford.edu

displaying stiff dynamics is difficult due to fundamental challenges in haptic control. High quality haptic interfaces should be simultaneously stable, free of noisy force signals that can generate unrealistic and unexpected audio or haptic sensations, and be accurately controlled to have the desired apparent mechanical properties.

In this paper, we examine a canonical one degree-of-freedom haptic display rendering a virtual spring and damper including the effects of device and human dynamics, sampling, quantization, time delay, and the low-pass filter operating on the device velocity estimate. We present conditions for various stability and quantization error regions, and include software to generate these regions as a function of system parameters, that output low-pass filter control parameters to achieve the largest renderable virtual stiffness.

A. Prior Work

This work builds upon significant prior research related to the stability and quantization error analysis of haptic displays.

Conditions for robust stability of a haptic display coupled to a human operator were established by Colgate and Brown [4] and Colgate and Schenkel [5]. They showed that to ensure stability of the haptic display when coupled to an arbitrary passive human impedance, the display must be *sampled data passive*, and that some physical damping is essential to dissipate energy leaks that occur due to sampling. We differentiate *sampled data passivity* from another similarly named concept we introduce in our analysis: *quantization error passivity*. Sampled data passivity speaks to coupled stability, and quantization error passivity concerns energy generation due to quantization error.

Sampled data passivity can be conservative compared to coupled stability [5]. For virtual spring and damper rendering, Hulin et al. [14] and Diaz and Gil [7] showed that with typical system parameters, sampled data passivity is extremely conservative compared to coupled stability, and further, a conservative condition for coupled stability is the stability of the uncoupled (no human interaction) display. For this reason, a practical robust stability condition for common applications is uncoupled stability. In these prior works, a low-pass filter operating on the velocity measurement was not included in the analysis; it is possible that an analysis including the low-pass filter would not have similar results.

Uncoupled stability boundaries were presented by Gil et al. [11], showing that virtual damping can expand the range of stable virtual stiffness. They showed that for typical system parameters, the maximum uncoupled stable stiffness is given by the ratio of total system damping to total system time delay. The stability boundaries were formed without modeling the low-pass filter, which could potentially affect stability.

Abbott and Okamura [1] and Diolaiti et al. [8] showed that position sensor quantization can cause persistent oscillations (limit cycles) for virtual spring rendering, and that some Coulomb friction is required

to prevent them. Their analyses are not applicable to an arbitrary virtual environment, e.g., the results do not apply to limit cycles due to virtual damping, which are particularly important in practice because damping feedback is formed by numerical differentiation of sensed position, magnifying quantization error. Further, Abbott and Okamura [1] and Diolaiti et al. [8] did not distinguish between different types of limit cycles due to quantization error, i.e., they did not analyze how the existence, or qualities, of limit cycles depend on the human impedance.

More aggressive low-pass filtering of the velocity estimate can mitigate the negative effects of quantization error, but can affect sampled data passivity/stability. Chawda et al. [2] presented a method to choose a low-pass filter cut-off frequency that maximizes the renderable range of virtual stiffness and damping for an identified model of a haptic display for an exogenous human interaction model using numerical simulation. Their analysis does not consider the effect of human coupling on stability or quantization error limit cycles, or present analytical sampled data passivity or quantization error results.

Griffiths et al. [12] and [13] described a fundamental trade-off between sampled data passivity/stability, quantization error noise rejection, and accuracy of the rendering, not related to the implementation of the haptic controller. These analyses did not present conditions for uncoupled stability and quantization error boundaries.

B. Contributions

In this paper, we examine virtual spring and damper rendering and construct explicit system parameter regions for sampled data passivity, uncoupled stability, quantization error passivity, malicious touch quantization error limit cycles, and uncoupled quantization error limit cycles.

Our key contribution is the following:

Key contribution: Virtual stiffness and damping haptic renderings are limited by either instability or quantization error noise. For essentially all rendering scenarios, uncoupled stability of the display ensures coupled stability to the human. Because humans are sensitive to quantization error induced “haptic kicks,” quantization error passivity is required for high quality. The intersection of both uncoupled stability and quantization error passivity is a complicated expression of system parameters, but can be generated numerically. We provide code (Extension 1 in the Appendix) to find control parameters for rendering the stiffest stable and quantization error noise-free haptic display as a function of system parameters.

We also make the following contributions:

- In addition to dimensionless inertia [5], we show that dimensionless damping describes the conservativeness of passivity compared to coupled stability. We show that for common system parameters, passivity is conservative (Section IV-B).
- For typical human coupling impedances, uncoupled (no human interaction) stability is conservative compared to coupled stability. In other words, our analysis on the relationship between uncoupled and coupled stability including a low-pass filter yields the same result as not considering the low-pass filter (Section IV-B).
- Low-pass filtering can significantly reduce the uncoupled stable region, but only if the cut-off frequency of the filter is lower than a frequency defined by the sum of the device and virtual damping over the device mass: $(b + B)/m$ (Section IV-C).
- Position quantization error can create error impulse forces or sustained vibrations, but cannot cause instability. In other words, if a system is bounded-input, bounded-output (BIBO) stable without quantization error, the system will still be BIBO stable with the addition of quantization error (Section V).
- The quantization error analysis applies to a *general* virtual environment (i.e., it is applicable to haptic rendering other than a virtual spring damper). We present sufficiency for quantization error passivity: Equation (44); necessity for no malicious touch limit cycles: Equation (52); and necessity for no uncoupled touch limit cycles: Equation (53) (Section V-C).
- We experimentally verify our theoretical stability and quantization error results with a Phantom Premium 1.5 haptic device (Section VI).

C. Paper Organization

The organization of the paper is as follows. In Section II, we propose models of a haptic display rendering a virtual spring damper. We consider human and device dynamics, quantization, sampling, time delay, and low-pass filtering of the velocity measurement. In Section III, we present stability and quantization error regions, and show an example highlighting how software included in the Appendix can be used to generate the renderable regions, and output control parameters for high performance. In Section IV, we analyze the relationship between sampled data passivity, coupled stability, and uncoupled stability, and show that low-pass filtering can significantly affect the sampled data passivity and stability of the system. In Section V, we analyze the error introduced to the system by quantization of the position measurement. We use a describing function analysis to predict limit cycles due to sensor resolution, isolate quantization error energy generated by the haptic display, and perform an energy analysis to establish various quantization error regions. In Section VI, the theoretical stability and quantization error conditions are compared to experimental data gathered with a Phantom Premium 1.5 haptic device.

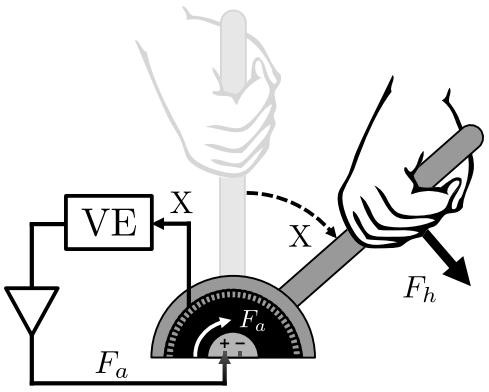

Fig. 1. Schematic of a human interacting with an impedance-type haptic device. The virtual environment, VE, is a map from sensed position to actuator force. In this paper, we consider a virtual environment of a spring and damper in parallel.

II. System Models

In this section we introduce system models for a human interacting with a haptic display, where the goal is to render a virtual spring and damper in parallel.

Three system models are introduced. One is a nonlinear hybrid model, which contains both linear and nonlinear, and both continuous and discrete, elements. This model is the closest to reality, in that the device friction is nonlinear, the position sensor measurement (usually corresponding an optical encoder) is quantized, and that the control of a physical haptic device is performed through a computer containing A/D (analog to digital) and D/A (digital to analog) components. Linear, entirely continuous and discrete models are also introduced. The continuous model is used for the identification of important parameters with respect to stability, and examining quantization error limit cycles. The discrete model is used to generate stability and quantization error boundaries.

A. Nonlinear Hybrid Model

Figure 2 (a) shows the nonlinear hybrid model. We consider a haptic device described by a mass, m, viscous damper, b, and Coulomb friction, c, acted upon by two external forces: the force applied by the operator, $F_h(s)$, and the force applied by the actuator implementing the virtual environment, $F_a(s)$. The operator's dynamics are modeled by a mass-spring-damper,

$$Z_h(s) = \frac{F_h(s)}{V(s)} = m_h s + b_h + \frac{k_h}{s} \tag{1}$$

where m_h, b_h and k_h are non-negative values corresponding to the human mass, damping, and stiffness, respectively. This model of human impedance represents the non-volitional biomechanics which are important for stability. Human dynamics can change significantly, from no human interaction, to light

(a) Nonlinear hybrid model

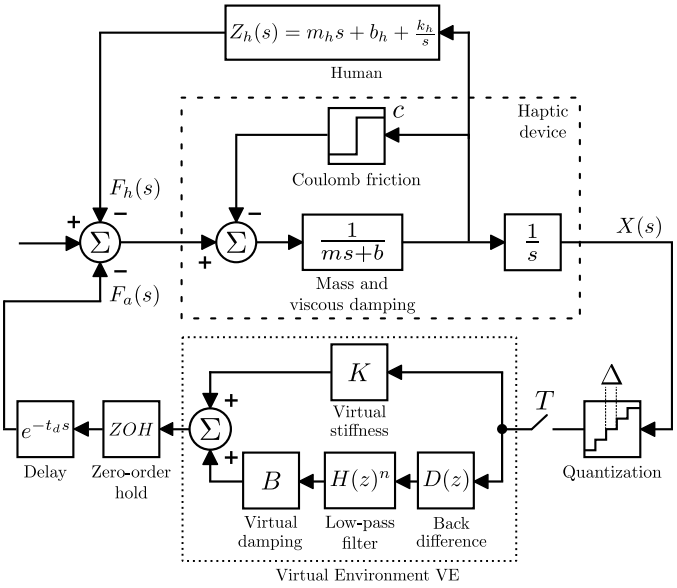

(b) Linear continuous model

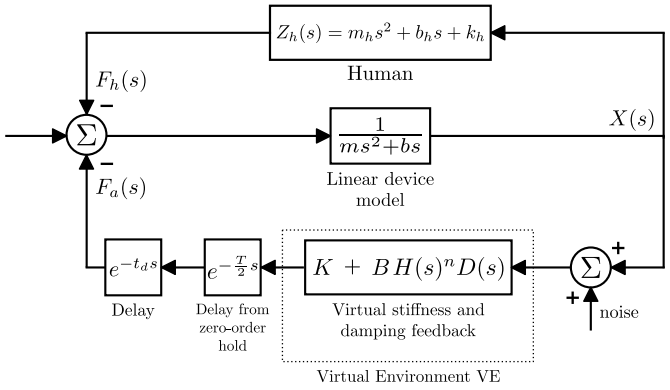

(c) Linear discrete model

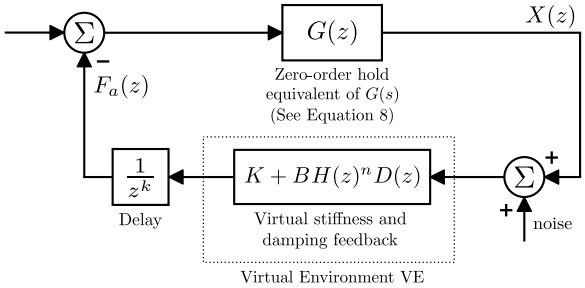

Fig. 2. Models used for the system. (a) The *nonlinear hybrid model* (Section II-A) considers human and device dynamics, quantization, sampling, ZOH, and time delay. (b) The *linear continuous model* (Section II-B) is created from the nonlinear hybrid model by omitting the nonlinear elements (Coulomb friction and quantization), and converting the discrete elements to continuous ones. (c) The *linear discrete model* (Section II-C), which has the same input-output characteristics as the linear hybrid model at sample times.

and heavy grasping. Because human dynamics are a function of user size, grip, and co-contration (i.e. the tensing of one's muscles) it will be most relevant to consider the set of likely human impedances.

The system is equipped with only one sensor measuring the position of the mass, $X(s)$, which is quantized with resolution Δ, and then sampled with a constant sampling period of T. To obtain an estimate of the velocity of the device, the sampled position measurements go through a discrete back differencing operator,

$$D(z) = \frac{(z-1)}{Tz}, \tag{2}$$

and then n first-order discrete low-pass filters,

$$H(z) = \frac{(1-e^{-\omega_0 T})z}{z-e^{-\omega_0 T}}, \tag{3}$$

where ω_0 (rad/s) represents the cut-off frequency of the low-pass filter. Other filters could be used; we chose one of the simplest possible filters to provide information about baseline performance. The force of the actuator is the sum of the virtual spring and damper forces. It is held constant for the duration of the sampling period with a zero-order hold (ZOH), resulting in a continuous-time staircase signal. To model time delayed actuator forces due to amplifier dynamics or transport time, the actuator force is delayed by t_d.

$$F_a(s) = e^{-t_d s}\, ZOH\{\, [K + BH(z)^n D(z)]\, \hat{X}(z)\}, \tag{4}$$

where $\hat{X}(z)$ is the quantized position measurement.

Figure 3 shows the quantization of true position, x, to estimated quantized position, $\hat{x}$. The mapping depends on the initialization of the system parametrized by $\kappa \in \mathcal{R}[0,1]$. Our analysis considers κ directly.

B. Linear Continuous Model

The entirely linear continuous model shown in Figure 2(b) approximates the nonlinear hybrid system shown in Figure 2(a). The linear continuous model is desirable because of its tractability for a describing function analysis and finding important parameters with respect to stability using conventional linear control systems analysis. The stability of the two systems are similar, but not identical.

To represent the system linearly, the Coulomb friction of the device is removed, and the quantization element is replaced with additive noise. To represent the system continuously, the discrete elements are converted to continuous ones. The continuous representation of $D(z)$, $D(s)$, is an exact derivative

$$D(s) = s. \tag{5}$$

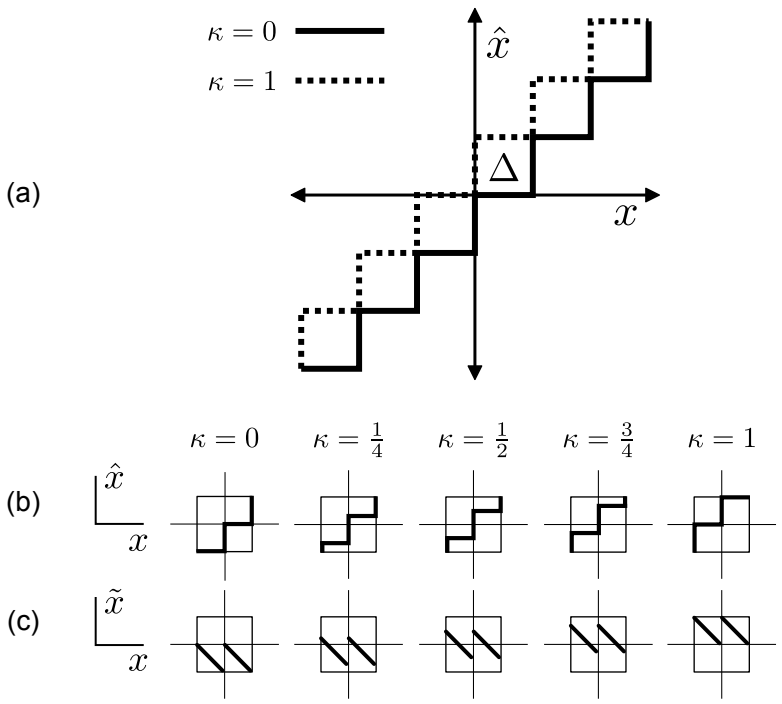

Fig. 3. Quantization maps true position, x, to estimated quantized position, $\hat{x}$, with quantization resolution, Δ, depending on the initialization parameter $\kappa \in \mathcal{R}[0, 1]$. (a) Quantization mapping occurs between two extremes described by $\kappa = 0$ and $\kappa = 1$. (b) Quantization mapping for various κ. (c) Quantization error, $\tilde{x} = \hat{x} - x$, for various κ.

The continuous representation of $H(z)$, $H(s)$, is a first-order low-pass filter with cut-off frequency ω_0 (rad/s) with unity gain at DC

$$H(s) = \frac{\omega_0}{s + \omega_0}. \tag{6}$$

The zero-order hold is modeled as a time delay equal to half the sample period

$$\text{ZOH} \rightarrow e^{-\frac{sT}{2}}. \tag{7}$$

The force of the actuator is

$$F_a(s) = e^{-(T/2+t_d)s} \ [K + BH(s)^n D(s)] \ X(s). \tag{8}$$

C. Linear Discrete Model

We also represent the system with the entirely linear discrete model shown in Figure 2(c). The linear discrete model is useful for stability and quantization error analyses in which the discrete elements can be considered explicitly. The linear discrete model is made linear from the hybrid model by the same steps taken to make the continuous system linear. To make the system discrete, the continuous elements in the linear hybrid model are replaced. First, a transfer function from $F_a(s)$ to $X(s)$, $G(s)$, is formed

combining only the continuous elements into a single transfer function,

$$\frac{F_a(s)}{X(s)} = G(s) = \frac{1}{(m+m_h)s^2 + s(b+b_h) + k_h}. \tag{9}$$

Then, the ZOH, $G(s)$, and the sample elements are converted into a discrete element, $G(z)$, using a zero order hold equivalent, [10],

$$G(z) = \frac{z-1}{z}\mathcal{Z}\left\{\frac{G(s)}{s}\right\}. \tag{10}$$

The continuous delay element is replaced by a discrete one,

$$e^{-t_d s} \rightarrow \frac{1}{z^k}, \tag{11}$$

where k is a nonnegative integer representing the length of the delay in number of sample times.

The force of the actuator is

$$F_a(z) = \frac{1}{z^k}\left[K + BH(z)^n D(z)\right] X(z). \tag{12}$$

The input-output properties of the linear continuous and discrete elements (at sample times) are the same. For this reason, the stability of the linear hybrid and discrete models are identical.

III. Stability and Quantization Error Regions

In this section, we present the main results for rendering a virtual spring and damper. First, we show qualitative stability and quantization error regions in the virtual stiffness and damping (K-B) plane, and reference the sections in the paper that show them quantitatively. Then, we describe conditions for virtual spring and damper accuracy, i.e., conditions in which the closed-loop rendered dynamics are similar to the desired dynamics. Finally, we generate the stability and quantization error intersection regions for an example haptic display, highlighting how code Extension 1 in the Appendix can be used as a design tool. Using this approach, we find the system parameters to render the highest virtual stiffness for each region.

A. Stability Regions

An obvious requirement for the haptic display is stability. This implies that the haptic feedback loop does not create exponentially growing oscillations. Figure 4 shows stability regions, denoted by a letter.

A: sampled-data passive (Section IV-A)

The haptic display is *sampled-data passive*. When coupled to *any* passive human impedance, the coupled system is guaranteed stable. In this region, no net energy generation from sample-and-hold dynamics are possible.

B: uncoupled stable (Section IV-D)

The haptic display is *uncoupled stable*. In other words, the display is stable for no human

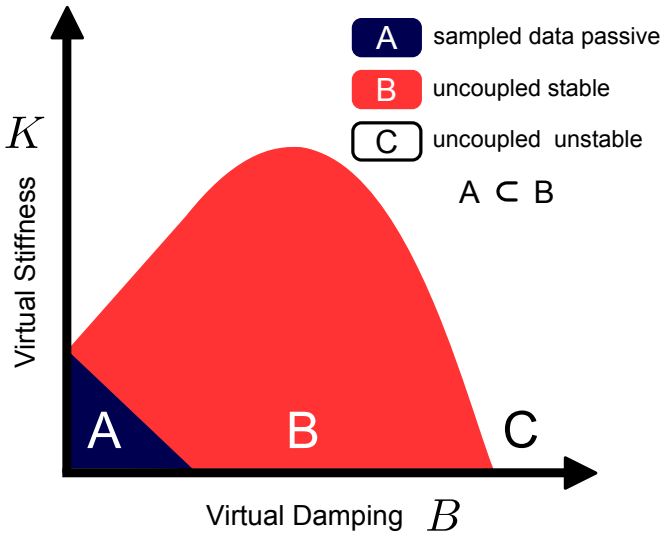

Fig. 4. Qualitative stability regions in the virtual stiffness damping (K-B) plane. In region A, the haptic display coupled to any passive human impedance is stable. In region B, the uncoupled (no human interaction) display is stable. Quantitative passivity and uncoupled stability plots are shown in Figures 9 and 13, respectively.

interaction. In section IV-B we show that for typical system parameters, the haptic display is insensitive to human coupling instability, so this region serves as a practical stability boundary for common applications. Here it is possible for the display to generate energy from sample-and-hold dynamics.

C: uncoupled unstable (Section IV-D)

The haptic display is *uncoupled unstable*. For no human interaction, the display will have exponentially growing oscillations. In this region, the display is expected to continuously generate energy due to sample-and-hold dynamics.

B. Quantization Error Regions

High quality haptic rendering should be free of unnatural feeling impulses or vibrations that can be caused by quantization error. Unlike instability oscillations, quantization error oscillations are bounded. However, in some cases, the bound can be very large. Figure 5 shows the quantization error regions, denoted by a number.

1: quantization error passive (Section V-C1)

The haptic display is *quantization error passive*. No net energy can be generated from quantization error over any time period for arbitrary human interaction.

2: quantization error active (Section V-C1)

The haptic display is *quantization error active*. The display can generate energy due to quantization error for some sample periods, but may dissipate energy over all sample periods.

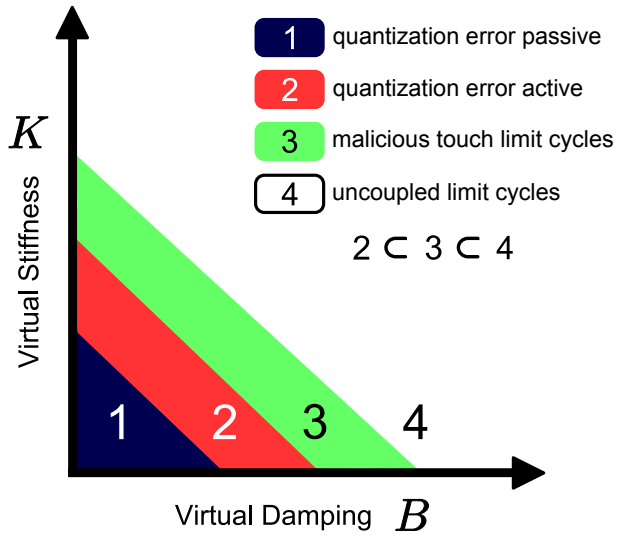

Fig. 5. Qualitative quantization error regions in the virtual stiffness damping (K-B) plane. In region 1, the haptic display cannot generate energy due to quantization error over any sample period; in region 2, it can. In region 3 a "malicious" user can elicit limit cycles, and in region 4, the uncoupled display is expected to have limit cycles. Quantitative quantization error plots are shown in Figure 18.

3: malicious touch limit cycles (Section V-C2)

The haptic display can have sustained oscillations (limit cycles) for human interaction in which the user acts with "malicious touch" to maximize the energy extraction due to quantization error. Here the haptic display can continuously generate energy due to quantization error.

4: uncoupled limit cycles (Section V-C3)

The uncoupled (no human interaction) haptic display is expected to have sustained oscillations (limit cycles). Here the haptic display can continuously generate energy due to quantization error.

C. Accuracy

We are interested not only in stability and quantization error, but also in the accuracy of the haptic rendering. In general, the *rendered* or *actual* dynamics will be different than the *commanded* or *desired* dynamics. In other words, the input-output properties of the closed-loop haptic display will not exactly match the haptic control law; the closer the rendered and desired dynamics, the more accurate the display.

A full accuracy analysis for virtual spring damper rendering is performed in [6]. For completeness, we present the key results for closed-loop stiffness and damping rendering.

- accuracy depends on the human interaction frequency f_i. For low f_i, accuracy is high: the majority of the rendered force is from the haptic control law. For high f_i, acccuracy is low: the majority of the rendered force is from the haptic device dynamics.
- the effective stiffness bandwith is $\sqrt{K/m}$ rad/s.

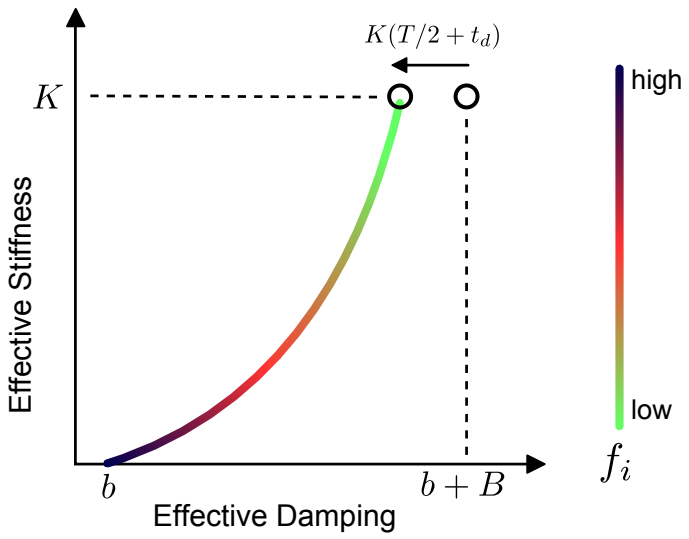

Fig. 6. Effective stiffness and damping [6], as a function of interaction frequency f_i. For low interaction frequencies, the haptic display is accurate: effective stiffness and damping are close to the desired stiffness and damping. However, as f_i increases, the display is less accurate.

- the effective damping bandwith is ω_0 rad/s.
- total time delay, $T/2 + t_d$, reduces effective damping by $K(T/2 + t_d)$, but does not significantly change effective stiffness.

Figure 6 shows the *rendered* effective stiffness and damping of the haptic display as a function of interaction frequency.

D. Design Guidelines

Based on these results, we present our suggestions for designing stiff dynamics on impedance type haptic displays using virtual stiffness and damping.

- The rendering will be limited by either instability or by noise due to quantization error. Adding virtual damping can increase stability, but also increases quantization error noise, so the problem of rendering the highest possible stiffness is a high dimensional control problem.
- For relevant human interaction scenarios, an uncoupled stable haptic display implies the stability of the coupled display-human system. This greatly simplifies the stability analysis because it removes consideration of human.
- Haptic displays that are quantization error active can render "haptic kicks:" force pulses that a human can perceive. Haptic displays with malicious touch or uncoupled limit cycles are capable of vibrating continuously. Because humans are sensitive to force pulses and vibrations, quantization error passivity is desired for a high quality rendering.
- Extension 1 in the Appendix can be used to generate control parameters for a maximally stiff, robustly

TABLE I
MAXIMUM K IN EACH REGION

	$K_{\max}$ (N/m)	B (Ns/m)	w_0 (rad/s)	n (-)
A1	143	0	–	–
B1	1063	5.26	314	3
B2	1892	14.74	503	4

stable, quantization-error-noise-free, haptic rendering by finding the intersection of uncoupled stability and quantization error passivity regions.

E. Example Application

Here we present a quantitative example showing the intersection of stability and quantization error regions using Extension 1 in the Appendix for a haptic display rendering a virtual spring and damper.

Because we present three stability regions, and four quantization error regions, there are twelve possible stable and quantization error intersection regions. All twelve regions can be generated, but for this example, we show only the most relevant regions for common applications:

A1 sampled data passive and quantization error passive.

B1 uncoupled stable and quantization error passive.

B2 uncoupled stable and quantization error active.

We consider a haptic system with "fixed" system parameters: $m = 250$ g, $b = 0.5$ Ns/m, $c = 0.1$ N, $\Delta = 0.00005$ m, $T = 0.001$ s, and $t_d = 0.003$ s. These parameters are determined by hardware, and are not easily changed. The values were chosen to represent currently existing haptic devices, mechatronic interfaces, and amplifier dynamics [8, 11, 2]. We consider "control" parameters: K, B, f_0, and n; these parameters are determined by software and are easily manipulated.

Figure 7 shows the A1, B1, and B2 regions. The maximum virtual stiffnesses for each region, and the control parameters to achieve them, are given in Table I. The control parameters were found by gridding the parameter space, and finding the highest virtual stiffnesses for each region which satisfied the region's criteria. Note that Figure 7 shows the *commanded* stability and quantization error intersection regions. In some haptic display cases, e.g., commanding large virtual damping which requires aggressive low-pass filtering to reduce the effect of quantization error noise, the display may be inaccurate [6].

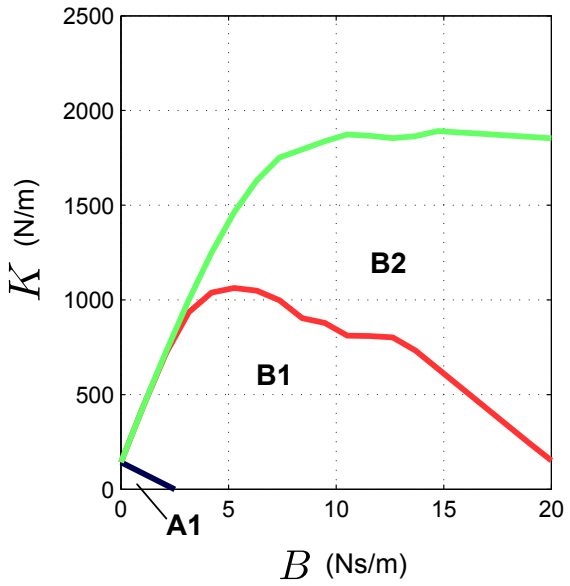

Fig. 7. The stability and quantization error intersection regions of the example haptic display over the span of the parameters of the low-pass filter, i.e., for each point in a region, there exists a cut-off frequency w_0, and filter order n, such that the point is in the region. The regions are *under* the curves.

IV. System Sampled Data Passivity and Stability

In this section we analyze the passivity and stability of the system shown in Figure 2.

First, we present conditions for *sampled-data* passivity of a haptic display rendering virtual stiffness and damping. This establishes sufficient and necessary conditions for the stability of the display when coupled to a passive, but otherwise arbitrary, human impedance.

Then, because sampled-data passivity can be conservative compared to coupled stability considering the likely set of human coupling impedances, we examine the relationship between sampled-data passivity and stability with various coupling impedances. We show that two factors determine the conservativeness of sampled-data passivity: dimensionless inertia, and dimensionless damping. For common system parameters, characterized by low sample times ($T \leq 0.001$ s) and non-aggressive low-pass filtering ($\omega_0 \gg b/m$), sampled-data passivity is extremely conservative. Further, we show that for typical models of human impedances, the uncoupled (no human impedance) stability region is a subset of the human impedance coupling region. Because of this, analyzing the uncoupled stability of the system is a practical way to establish stability of the haptic display for typical applications.

Concentrating on uncoupled stability, we analyze the qualitative effect of system parameters on stability. We show that the low-pass filter cut-off frequency and low-pass filter order can both significantly reduce stability if the filtering is aggressive, i.e., low-pass filtering reduces the uncoupled stable region if the cut-off frequency of the filter is lower than a frequency defined by the sum of the device and virtual

damping over the device mass: $(b+B)/m$.

Finally, we generate quantitative uncoupled stability boundaries. These serve as a design tool for creating stable spring damper haptic displays.

A. *Sampled-Data Passivity*

Guaranteeing the stability of a haptic display coupled to a potentially large range of dynamics can be accomplished through passivity. If the haptic display is shown to be passive, and the user is assumed strictly passive, the feedback interconnection of the two is passive, and therefore necessarily stable [3]. In point of fact, the user violates passivity due to volitional feedback; however, in practice it is sufficient to assure that the passive bio-mechanics are stable when coupled to the haptic device [13].

Here we use the general passivity theorem of Colgate and Schenkel [5] to generate passivity bounds for a haptic display rendering virtual stiffness and damping. The theorem applies to the uncoupled linear hybrid model (Figure 2(a) without Coulomb friction, quantization, and the human). It states that a sufficient and necessary condition for passivity is

$$b \; > \; \frac{T}{2}\frac{1}{1-cos(\omega T)}\mathfrak{Re}\{(1-e^{j\omega T})\,Q(e^{j\omega T})\,e^{-jwt_d}\} \tag{13}$$

$$\text{for} \quad 0 \leq \omega \leq \frac{\pi}{T} \tag{14}$$

where $Q(z)$ represents the discrete time haptic control law. We consider the virtual spring damper control law, including low-pass filtering and time delay,

$$Q(z) = [K + BD(z)H(z)^n]z^{-k}, \tag{15}$$

where k is a nonnegative integer representing the length of the delay in units of sample times.

Combining Equation (15) and Inequality (13), the sampled-data passivity condition can be rewritten as

$$b > K\left(\frac{T}{2}+t_d\right) + g\left(T, t_d, f_0, n\right)|B|\,, \tag{16}$$

where $g\left(T, t_d, f_0, n\right)$ is the "passivity damping coefficient." We could not find a tractable symbolic expression for $g\left(T, t_d, f_0, n\right)$, but it can be generated numerically. Figure 8 displays the passivity damping coefficient as a function of sample time, cut-off frequency, and filter order. For negative virtual damping, the passivity damping coefficient, is unity regardless of the sample time, time delay, or parameters of the low-pass filter. For positive virtual damping, in contrast, the passivity damping coefficient depends on all parameters: the passive range of positive virtual damping is expanded for smaller sample times, lower time delay, and lower cut-off frequency.

For no time delay, and no low-pass filter, Inequality (16) collapses to the well-known sampled data passivity condition, [5]:

$$b > \frac{KT}{2} + |B|\,. \tag{17}$$

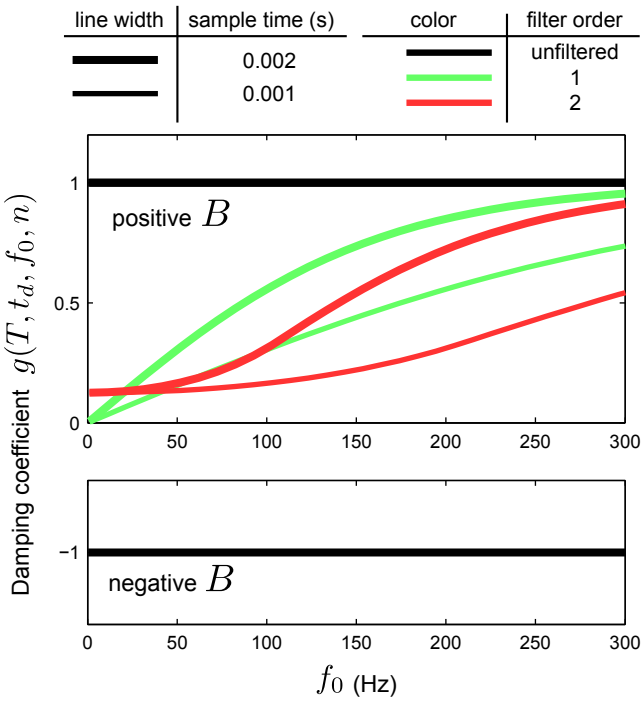

Fig. 8. The virtual damping coefficient $g\,(T, t_d, f_0, n)$ as a function of sample time, filter order, and cut-off frequency. For positive B, the coefficient is smaller for lower sample times, and cut-off frequencies (corresponding to larger regions of virtual damping passivity), but not for negative B, where the parameters do not affect the coefficient.

Figure 9 shows the sample-data passivity boundaries in the virtual stiffness and damping plane (K-B width) for device damping $b = 0.1$ Ns/m, sample time $T = 0.001$ s, and no time delay. We call this region K-B width as a connection to the Z-Width of a haptic display. Although Z-width is a general term spanning all impedances, it has generally been discussed as relating to haptic rendering of a virtual spring damper. We imagine Z-Width representing the infinite dimensional sampled data passive impedances of a haptic display, where K-Width is the passive range of pure virtual stiffness, B-Width is the passive range of pure virtual damping, M-Width is the passive range of pure virtual mass, etc.

Adding virtual damping *reduces* the sampled data passive range of virtual stiffness. We will find that generally virtual damping has the opposite effect on uncoupled stability: adding virtual damping *expands* the uncoupled stable range of virtual stiffness.

B. Relationship Between Sampled-Data Passivity, Coupled Stability, and Uncoupled Stability

The virtual stiffness and damping values that are sampled data passive, coupled stable for likely human impedances, and uncoupled (no human interaction) stable, can be different for various system parameters.

Inequality (16) is a sufficient *and necessary* condition for coupled stability when the haptic display is connected to a passive system, i.e., if the display is non-passive, there exists a passive coupling impedance

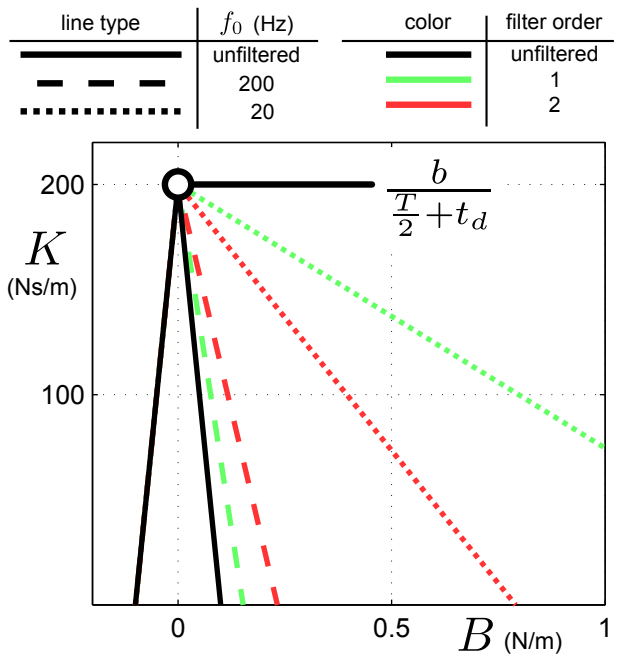

Fig. 9. K-B width: the sampled data passive virtual stiffness and damping region. The passive regions are *under* the curves. More aggressive filtering, characterized by lower cut-off frequency and higher filter order, allows a larger range of positive virtual damping, but not negative virtual damping. The largest passive virtual stiffness is achieved for no virtual damping.

such that the coupled system is unstable [5]. However, because the set of impedances that a human can display are a subset of all passive ones, Inequality (16) can be overly conservative.

Colgate and Schenkel [5] showed that "dimensionless inertia," m/bT, is a measure of the conservativeness of passivity compared to coupled and uncoupled stability: the larger the dimensionless inertia, the more conservative. Because most impedance-type haptic displays feature small sample times ($T \leq 0.001$ s), the dimensionless inertia is large ($m/bT \geq 1000$), and passivity is extremely conservative compared to coupled stability [11].

Our analysis, which models the low-pass filter of the velocity estimate, reveals that conservativeness of passivity also depends on "dimensionless damping," $b/m\omega_0$. Figure 10 shows the stable regions in the K-B plane for four possible human interactions: (1) any passive, (2) uncoupled, (3) spring impedance, and (4) spring-damper impedance, with dimensionless inertia $m/bT = 1000$. Informally, the spring can be interpreted close to a "worst-case," human coupling environment [5], and the spring-damper as a more realistic one because human bio-mechanics necessarily add damping when adding stiffness [8]. The larger the dimensionless damping, the less conservative passivity is compared to the other coupling impedances. This result reveals that low-pass filtering powerfully affects the conservativeness of passivity compared to coupled stability: the more aggressive the filtering, the less conservative passivity is. In most cases, the low-pass filter cut-off frequency, ω_0, is chosen sufficiently higher than b/m to satisfy stability and

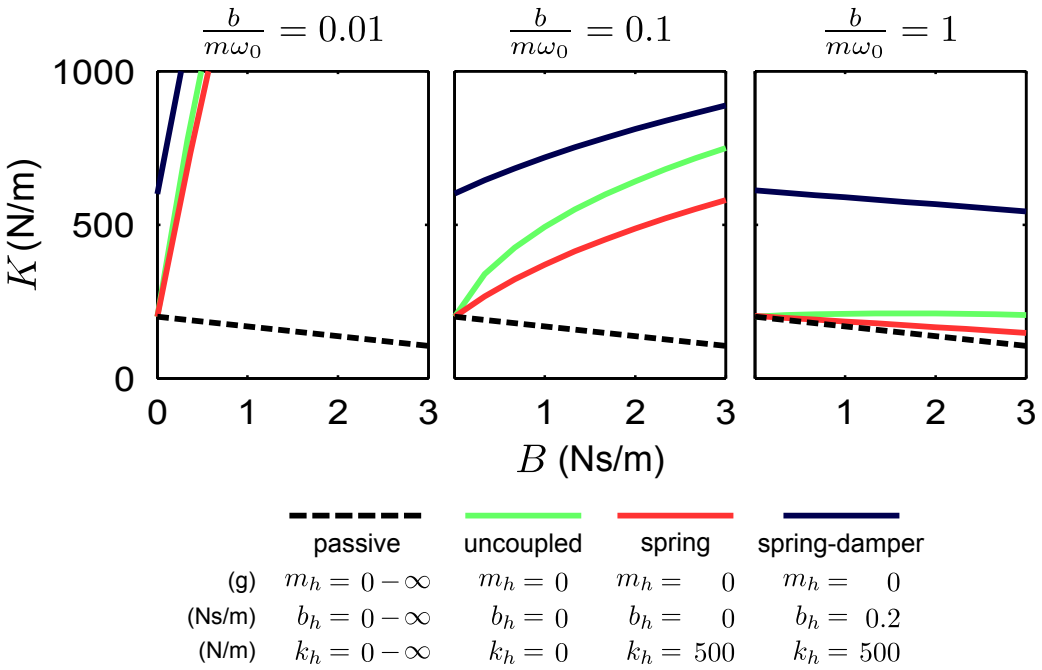

Fig. 10. The stable virtual stiffness and damping region with different coupling impedances for various dimensionless damping $b/m\omega_0$. The stable regions are *under* the curves. For high dimensionless damping, the passive region is similar to the spring and uncoupled stability regions, but not for low dimensionless damping. For the cases, the uncoupled stability region is a subset of the spring damper coupling stability region.

accuracy objectives, so passivity is very conservative.

For the cases in Figure 10, the uncoupled stability region is a subset of the spring-damper stability region. This analysis suggests that for common human interaction, the human *aids* stability, i.e., the uncoupled haptic display has a "baseline" stability that can be improved by the user. Therefore, to analyze the stability of virtual spring and damper rendering with typical human interaction, we can consider the stability of the uncoupled ($m_h = b_h = k_h = 0$) system. This technique has previously been used to analyze virtual spring and damper rendering stability, where for reasonable human coupling conditions, the human is assumed to aid stability [11], [14].

C. Effects of Parameters on Uncoupled Stability

Here we focus on uncoupled stability ($m_h = b_h = k_h = 0$), and analyze the characteristic equation of the continuous system shown in Figure 2(b) to find important parameters for stability. By examining how Bode or Nyquist plots change with system parameters, we observe the effect of the parameters on stability.

The characteristic equation of the system is

$$1 + L(s), \tag{18}$$

where

$$L(s) = \frac{KG(s)e^{-s\left(\frac{1}{2}T+t_d\right)}}{1 + G(s)D(s)H(s)^n Be^{-s\left(\frac{1}{2}T+t_d\right)}} \tag{19}$$

and $G(s)$, $D(s)$, and $H(s)$ are defined by Equations (9) (5) and (6) respectively.

It is convenient to define ω^* as the frequency at which the phase of $L(s)$ is $-180°$. The stability of the system is determined by the value of the gain margin of $L(s)$. The gain margin, GM, is defined to be

$$GM = \frac{1}{|L(\omega^*)|}. \tag{20}$$

A gain margin greater than one corresponds to a stable system, and a gain margin of less than one corresponds to an unstable system. Each parameters affects the gain margin differently.

- m does not significantly affect the gain margin.
- b increases the gain margin.
- K is a direct gain of the system; changing it directly affects the gain margin. There exists a maximum stable positive value of K.
- B affects the margin differently depending on its sign.
  - positive B increases the gain margin until B reaches a critical value, B^*, and then reduces the margin.
  - negative B reduces the gain margin.
- ω_0 only significantly affects the gain margin if $\omega_0 < \bar{\omega} = \frac{b+B}{m}$, which represents a pole of the system with no filter. If $\omega_0 < \bar{\omega}$, then the gain margin is increased for increasing ω_0, corresponding to less aggressive filtering.
- n only significantly affects the gain margin if $\omega_0 < \bar{\omega}$. If $\omega_0 < \bar{\omega}$, the higher the filter order, the lower the gain margin.
- T and t_d affects how quickly phase lag is added to the system. As T and t_d increase, the gain margin decreases.

The effects of the these system parameters on the gain margin of $L(s)$ is summarized in Table II.

Figure 11 shows how $L(s)$ varies with cut-off frequency and filter order for $m = 100$ g, $b = 0.1$ Ns/m, and $B = 1$ (Ns/m). If $\omega_0 \gg \bar{\omega} = \frac{b+B}{m}$, the loop polynomials are similar to the loop polynomial with no filter, i.e., low-pass filtering does not affect stability. However, if $\omega_0 < \bar{\omega}$, low-pass filtering affects stability: a lower cut-off frequency, ω_0, or a higher filter order, n, (corresponding to more aggressive filtering), makes the system less stable.

Figure 12 shows the Nyquist plots for systems with different virtual damping B, for two cut-off frequency conditions: $\omega_0 > \bar{\omega}$, and $\omega_0 < \bar{\omega}$ for $m = 100$ g and $b = 0.1$ Ns/m. For $\omega_0 > \bar{\omega}$, corresponding to light filtering, the larger the virtual damping, the larger the gain margin, i.e., virtual damping *increases*

TABLE II

EFFECT OF PARAMETERS ON GAIN MARGIN OF $L(s)$

Parameter	Gain Margin
m	-
b	$\Uparrow$
K	$\Downarrow$
positive B $(B < B^*)$	$\Uparrow$
positive B $(B > B^*)$	$\Downarrow$
negative B	$\Downarrow$
ω_0 $(\omega_0 < \bar{\omega})$	$\Uparrow$
ω_0 $(\omega_0 \gg \bar{\omega})$	-
filter order n $(\omega_0 < \bar{\omega})$	$\Downarrow$
filter order n $(\omega_0 \gg \bar{\omega})$	-
T, t_d	$\Downarrow$

Table entries represent the general change in gain margin as the parameters are *increased*. $\bar{\omega} = \frac{b+B}{m}$ represents a pole of the system with no filter.

the stable range of virtual stiffness for non-aggresive filtering. For $\omega_0 < \bar{\omega}$, corresponding to aggressive filtering, the larger the virtual damping, the smaller the gain margin, i.e., virtual damping *decreases* the stable range of virtual stiffness for aggresive filtering.

D. Uncoupled Stability Boundaries

Here we form analytical stability boundaries for the uncoupled haptic display. The uncoupled discrete model shown in Figure 2(c), ensuring the stability of the uncoupled non-linear hybrid model in Figure 2(a), will be stable if and only if

$$GM[L(z)] > 1, \tag{21}$$

where

$$L(z) = \frac{KG(z)z^{-k}}{1 + G(z)D(z)H(z)^n Bz^{-k}} \tag{22}$$

$G(z)$, $D(z)$, and $H(z)$ are defined by equations (10), (2), and (3), respectively, n is the filter order, and k is a non-negative integer representing the time delay in units of the sample time T. The gain margin of $L(z)$ can be evaluated straightforwardly for given system parameters.

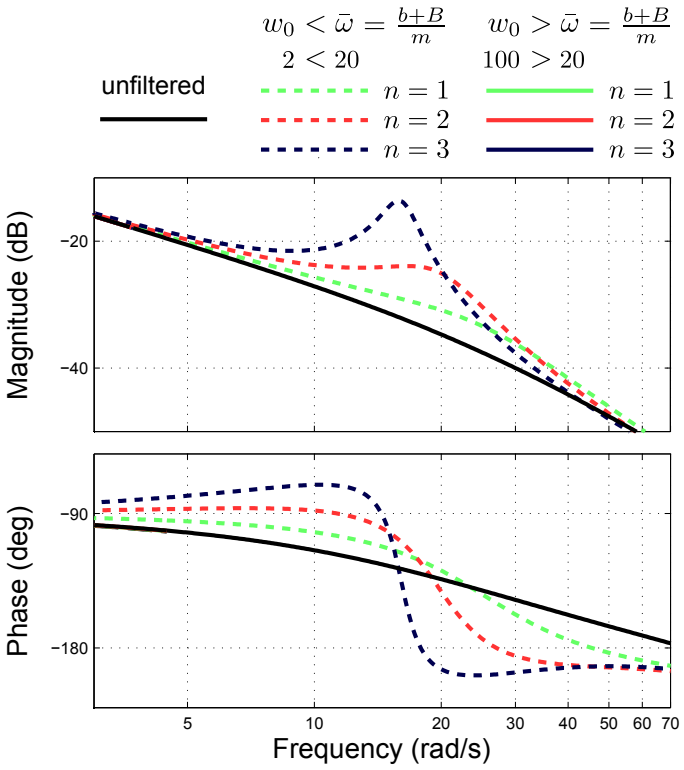

Fig. 11. Bode plots of $L(s)$ for different cut-off frequencies and filter orders. The stability of the unfiltered and filtered systems are significantly different only if $\omega_0 < \bar{\omega} = \frac{b+B}{m}$. If $\omega_0 < \bar{\omega}$, the system is less stable for decreasing cut-off frequency and increasing filter order.

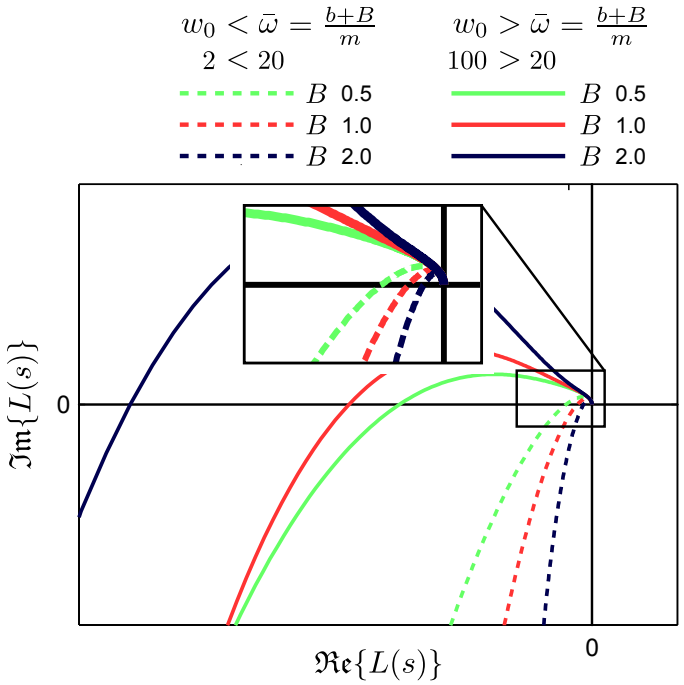

Fig. 12. Nyquist plots of $L(s)$ with varying virtual damping B for light and aggressive low-pass filtering. Increasing the virtual damping aids stability for light filtering, but hinders stability for aggressive filtering.

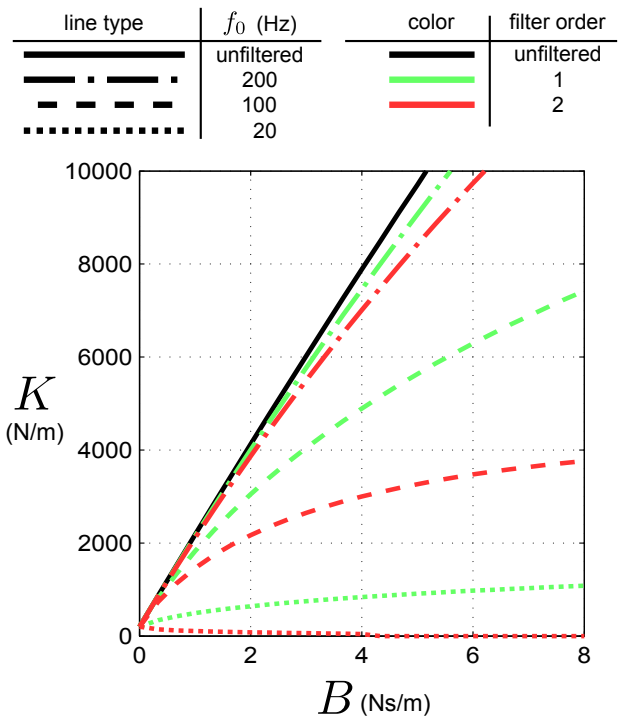

Fig. 13. Uncoupled stable regions of virtual stiffness and damping. The stable regions are *under* the curves. As the cut-off frequency is reduced, or the filter order is increased (corresponding to more aggressive low-pass filtering), the stable region decreases.

Figure 13 shows the stability boundaries in the K-B plane for various cut-off frequencies and filter orders $m = 100$ g, $b = 0.1$ Ns/m, and no time delay. The cut-off frequency can have a strong effect on stability: for high cut-off frequency, corresponding to light filtering, the stability of the system is similar to the stability of the system with no low-pass filter, for low cut-off frequency, corresponding to strong filtering, the stable range of virtual stiffness and damping reduces significantly. Increasing the filter order reduces the range of stable values.

Figure 14 shows the stability boundaries in the K-B plane for varying amounts of time delay for low and high cut-off frequency for a second order low-pass filter ($n = 2$). Time delay in the haptic feedback loop strongly reduces the stable ranges of virtual stiffness and damping.

Our results show that if the dimensionless inertia is sufficiently large, and the dimensionless damping is sufficiently small, the general stability condition, Inequality (21), is the same as the uncoupled stability condition reported for unfiltered velocity, [11]

$$b + B > K\left(\frac{T}{2} + t_d\right). \tag{23}$$

When these conditions are satisfied, virtual damping *increases* the range of uncoupled virtual stiffness. This is in contrast to sampled data passivity, Inequality (16), where virtual damping *reduces* the range of passive virtual stiffness.

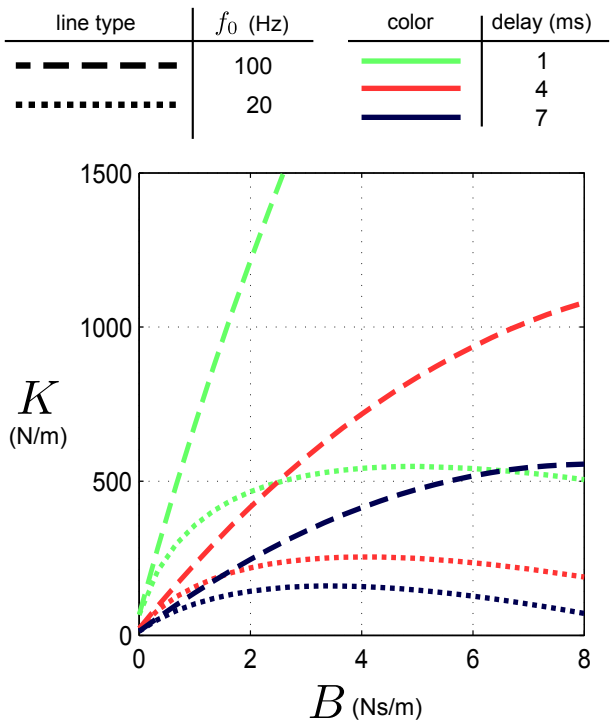

Fig. 14. Uncoupled stability regions with time delay. The stable regions are *under* the curves. Time delay severely hinders stability; especially for non-aggressively filtered virtual damping.

V. Quantization Error Analysis

In this section we analyze the error introduced by quantization of the position measurement.

Because quantization introduces finite error, it cannot cause a stable system to go unstable in the BIBO sense [9]. However, the error can cause the haptic display to generate energy. In some cases, the error can be large enough that the noise introduced in the haptic display causes it to shake violently, and practically speaking the system is "unstable."

First, we predict the existence and qualities of sustained oscillations (limit cycles) with a describing function analysis of quantization.

Then, we show that the total energy generated by the haptic display can be divided into two components: the energy generated from the haptic control law operating on true position, and the energy generated from the haptic control law operating on quantization error. This enables an analysis of the effect of quantization error on the system.

Finally, concentrating on the energy generated by quantization error, we analyze the net energy of the haptic display for various interaction scenarios. We establish a general sufficient and necessary condition for *quantization error passivity*: in which the haptic display is unable to generate energy due to quantization error over *any* sample period. We also establish necessary conditions for *continuous* energy generation considering unrestricted (malicious) and uncoupled device trajectories.

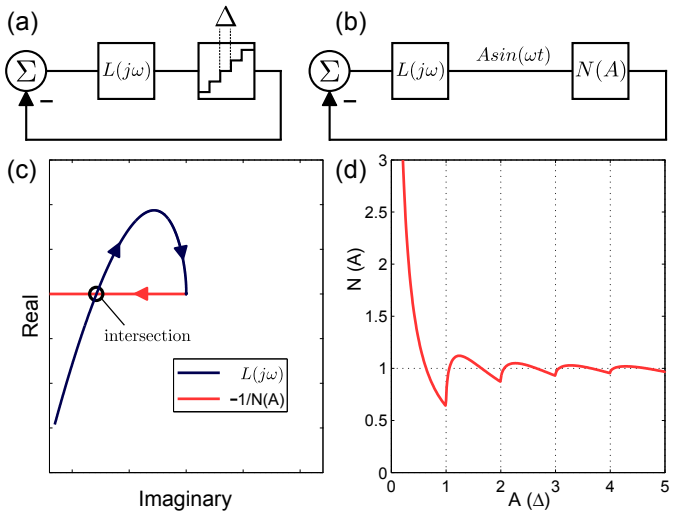

Fig. 15. (a) Block diagram of the lumped linear system and quantizer. (b) Block diagram of the system and quantizer describing function. c) Nyquist contour of $L(j\omega)$ without Coulomb friction showing the existence of limit cycles. The arrow of $L(j\omega)$ represent the direction of increasing ω, and the arrow of -$1/N(A)$ represent the direction of increasing A. (d) Quantizer describing function.

A. Describing Function Analysis

Describing function analysis [16] provides a tool to analyze "average" behavior in which the frequency, amplitude, and stability, of self-sustaining oscillations from quantization can be predicted.

Figure 15 shows the continuous system of Figure 2(b) with all the linear components lumped together and the quantizer in a feedback loop. $L(j\omega)$ is given by Equation (19).

If we assume a sinusoidal input to the quantizer of

$$A \sin \omega t, \text{ for } A > 0, \omega > 0, \tag{24}$$

then the input-output properties of the non-linear quantizer can be approximated by its linear describing function [16]. We approximate quantization for all initialization parameters κ, by quantization for $\kappa = 0.5$, whose describing function is given by

$$N(A) = \frac{2}{\pi A} + \frac{4}{\pi A^2} \sum_{l=1}^{\lfloor A \rfloor} \sqrt{A^2 - l^2}, \tag{25}$$

where A is the amplitude in quantization intervals [16]. Equation (25) is illustrated in Figure 15(d). Note that quantization is static and odd with respect to position, so $N(A)$ is real and not a function of frequency ω [15].

From the Nyquist criterion, sustained oscillations are predicted to occur (without Coulomb friction) if

$$L(j\omega)N = -1 \text{ for } A > 0, \omega > 0. \tag{26}$$

Figure 15 displays the Nyquist contour of $L(j\omega)$ for positive ω, and $-1/N(A)$ for positive A. Because

Condition (26) is satisfied, limit cycles are predicted to occur. This confirms that "noise" limit cycles occur because of quantization and not Coulomb friction, in fact, we will find that Coulomb friction can actually prevent these limit cycles. The solution sets can be solved for two separate cases of the input amplitude to quantization.

The first case is large amplitude ($A > \Delta$), where $N(A)$ tends to unity. In this case, the limit cycles are unstable, and the analysis reduces to the standard Nyquist stability criterion which is covered in Section IV.

The second case is small input to the quantizer ($A < \Delta$), in which the limit cycles are stable. There is a unique frequency, ω^*, in which Condition 26 is satisfied

$$\omega^* = \omega \text{ such that } L(j\omega) = -1/N(A). \tag{27}$$

Real haptic systems, however, have Coulomb friction which may prevent these limit cycles, as well as change their frequency. It is possible to form a describing function for $L(j\omega)$ including Coulomb friction in which its effect can be analyzed directly [8]. This approach requires solving coupled nonlinear equations for which finding solutions, or guaranteeing that none exist, is difficult. In our analysis, this technique applied to virtual spring and damper rendering is prohibitively cumbersome, so instead we take another approach. Limit cycles can only occur if the energy created from quantization error is greater than the energy dissipated. If the energy dissipation of the robot is greater than the "quantization error energy" then limit cycles cannot occur, and quantization noise will not be a limiting factor for the haptic rendering.

B. Quantization Error Energy

Energy is generated by the haptic display from the control law operating on quantized measured position,

$$\hat{E}_{\text{gen}} = \sum_{i=0}^{\infty} \left(\int_0^T \hat{f}_{a,i}(\hat{x})\, \dot{x}\, dt \right), \tag{28}$$

where $\hat{E}_{\text{gen}}$ is the total energy generated, $\hat{f}_{a,i}$ is the force of the actuator for time period i, $\hat{x}$ is the quantized measured position, and $\dot{x}$ is the true velocity. The force of the actuator is held constant for each sample period from the zero-order hold.

Position quantization can be modeled as noise as shown in Figure 16. At each instant in time

$$\hat{x} = x + \tilde{x} \tag{29}$$

where x is the true position, $\hat{x}$ is the quantized measured position, and $\tilde{x}$ is the error. Because of this, the actuator force for each sample period i can be decomposed into two components

$$\hat{f}_{a,i}(\hat{x}) = f_{a,i}(x) + \tilde{f}_{a,i}(\tilde{x}), \tag{30}$$

(a)

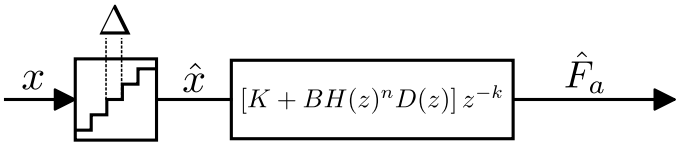

(b)

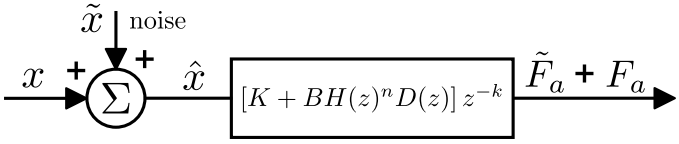

Fig. 16. Quantization error modeling. (a) Quantization operation: true position x is quantized with quantization interval Δ, to output quantized position $\hat{x}$, which propagates to produce actuator force derived from quantized position $\hat{F}_a$. (b) Quantization modeling: noise $\tilde{x} \in \mathcal{R}[\text{-}\Delta, \Delta]$ over all κ is added to the true position, which propagates to produce "noise" actuator force $\tilde{F}_a$.

where $f_{a,i}(x)$ is the force derived from true position, and $\tilde{f}_{a,i}(\tilde{x})$ is the force derived from quantization error. Plugging in Equation (30) into Equation (28), the total energy generated, $\hat{E}_{\text{gen}}$, can be decomposed as follows:

$$\hat{E}_{\text{gen}} = \sum_{i=0}^{\infty} \left(\int_0^T \hat{f}_{a,i}(\hat{x})\, \dot{x}\, dt \right), \tag{31}$$

$$= \sum_{i=0}^{\infty} \left(\int_0^T \left(f_{a,i}(x) + \tilde{f}_{a,i}(\tilde{x}) \right)\, \dot{x}\, dt \right), \tag{32}$$

$$= \sum_{i=0}^{\infty} \left(\int_0^T f_{a,i}(x)\, \dot{x}\, dt \right) + \sum_{i=0}^{\infty} \left(\int_0^T \tilde{f}_{a,i}(\tilde{x})\, \dot{x}\, dt \right), \tag{33}$$

$$= E_{\text{gen}} + \tilde{E}_{\text{gen}}, \tag{34}$$

where E_{gen} is the energy generated from true position, and $\tilde{E}_{\text{gen}}$ is the energy generated from quantization error.

Equation (34) allows an analysis of the energy generation of the haptic display due to quantization error decoupled from the energy generation derived from real position.

C. Quantization Error Energy Analysis

Here we consider the energy generated by the haptic display from quantization error, and the energy dissipated from the haptic device friction and damping. We establish conditions for net energy generation manifesting as force impulses or limit cycles for various human interaction scenarios.

The generated energy from quantization error is

$$\tilde{E}_{\text{gen}} = \sum_{i=0}^{\infty} \left(\int_0^T \tilde{f}_{a,i}(\tilde{x})\, \dot{x}\, dt \right) \tag{35}$$

where

$$\tilde{f}_{a,i}(\tilde{x}) = \sum_{k=-\infty}^{\infty} q(k)\tilde{x}(i-k). \tag{36}$$

The actuator force at time i, $\tilde{f}_{a,i}(\tilde{x})$, is the convolution sum the impulse response of the discrete-time haptic control law $Q(z)$, $q(k)$, with the position errors $\tilde{x}(k)$. Of course, for real-time haptic systems given by Figure 2, $Q(z)$ will be casual, that is, $q(k) = 0,\ \forall k < 0$. The impulse response of Q(z) can in general have an infinite number of non-zero terms, but for $Q(z)$ stable, and finite quantization error, the quantization error force given by Equation (36) will be finite.

The dissipated energy of the haptic display from Coulomb friction and viscous damping is

$$E_{\text{diss}}(x) = \sum_{i=0}^{\infty} \left(\int_0^T (c\,\text{sgn}(x) + b\,\dot{x})\ \dot{x}\,dt \right). \tag{37}$$

The difference between the quantization error and dissipation energy is the net energy of the display

$$E_{\text{net}} = \tilde{E}_{\text{gen}} - E_{\text{diss}}. \tag{38}$$

With respect to the trajectory of x from one sample time to the next, $\tilde{E}_{\text{gen}}$ is maximized, and E_{diss} is minimized, for monotonic trajectories with no stops of finite time [1]. Because of this, the nonlinear switching nature of Coulomb friction is removed. A lower bound on the energy dissipation from viscous damping is obtained from the Cauchy-Shwarz theorem. Therefore, an upper bound on the net energy generation from quantization error is

$$E_{\text{net}} = \tilde{E}_{\text{gen}} - E_{\text{diss}} \leq \tag{39}$$

$$\sum_{i=0}^{\infty} \left(\sum_{k=-\infty}^{\infty} q(k)\tilde{x}(i-k)|\delta x| - c|\delta x| - \frac{b}{T}|\delta x|^2 \right) \tag{40}$$

where δx represents the difference between true positions at the current and past sample period. Note that the net energy is a function of the true position at sample times only. Equation (40) is a general expression for the "net quantization error energy" of the haptic display in time.

1) Quantization error passivity: sufficiency for no net quantization error energy generation over any sample period: The maximum magnitude of the position error at each time step is a function of the quantization initialization parameter κ

$$\max|\tilde{x}| = \left[\frac{1}{2} + \left(\kappa - \frac{1}{2} \right) \right] \Delta. \tag{41}$$

Over all κ, the maximum magnitude of the position error is Δ. Because of this, the actuator force derived from quantization error at any sample time can be bounded

$$\sum_{k=-\infty}^{\infty} q(k)\tilde{x}(i-k) \leq \sum_{k=-\infty}^{\infty} |q(k)|\Delta = \|Q(z)\|_{\ell_1}\Delta, \tag{42}$$

where $\|Q(z)\|_{\ell_1}$ is the ℓ_1 norm on the discrete-time control law $Q(z)$ [17].

Plugging in Equation (42) into Equation (40), an upper bound for the net quantization error energy generation of the haptic display for a single sample period is

$$E_{\text{net}} \leq \|Q(z)\|_{\ell_1}\Delta|\delta x| - c|\delta x| - \frac{b}{T}|\delta x|^2. \tag{43}$$

As δx approaches zero, the energy dissipation from viscous damping is negligible compared to the energy dissipation from Coulomb friction. Therefore, for no net energy generation of the haptic display due to quantization error over any sample period we require

$$c > \|Q(z)\|_{\ell_1}\Delta. \tag{44}$$

This condition is sufficient, i.e., if Inequality (44) is satisfied, the haptic display cannot create energy due to quantization error over any sample period. For virtual spring and damper rendering, the condition for quantization error passivity is

$$c > \| \left[K + BD(z)H(z)^n\right] z^{-k} \|_{\ell_1} \Delta. \tag{45}$$

Inequality (45) provides an analytical expression for the virtual spring and damping values for which the quantization energy is guaranteed to be entirely dissipated by friction. Figure 17 shows the quantization error passivity region for $\Delta = 0.0001$ m, $T = 0.001$ s, and $c = 0.1$ N for various filter orders and cut-off frequencies.

2) Necessity for no continuous energy generation "malicious touch vibrations": Inequality (45) is a sufficient condition for no energy generation over *any* sample period. It is possible that the haptic display can generate energy over *some* sample periods, but dissipates energy on average over *all* sample periods.

In our analysis, we did not find a tractable sufficient and necessary condition for no continuous energy generation due to quantization error for a general haptic control law. Here, we present a necessary condition. In this scenario, the user acts in a way to extract as much energy as possible, so we call the user "malicious" [1].

A heuristic for maximizing the net energy generation of the haptic display in time is a trajectory which straddles the quantization boundary. For this trajectory, the energy dissipation of the display is only due to Coulomb friction (viscous damping becomes negligible), and the haptic control law operates on the largest possible magnitude of the quantization error.

The net energy over one cycle starting at one side of a quantization interval, traveling a small distance ϵ to other, and then returning to the original location is

$$E_{\text{net}} = \tilde{f}_{a,1}(\tilde{x})\epsilon + \tilde{f}_{a,2}(\tilde{x})\,(\text{-}\epsilon) - 2c\epsilon. \tag{46}$$

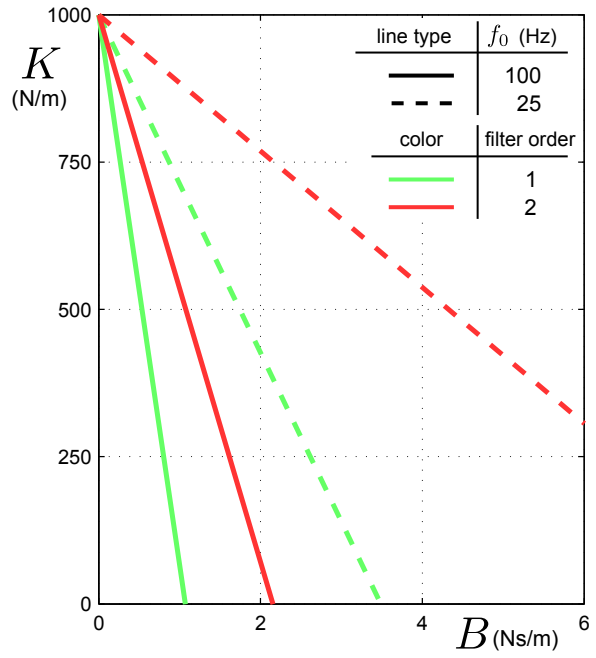

Fig. 17. The quantization error passive region for different low-pass filter orders and cut-off frequencies. The passive regions are *under* the curves. More aggresive low-pass filtering, characterized by higher filter orders, or lower cut-off frequencies, expands the quantization error passive region.

The position error, $\tilde{x}$, for this trajectory switches back-and-forth between $\kappa\Delta$ and $(\kappa-1)\Delta$. Therefore, we can write Equation (46) as

$$E_{\text{net}} = [q(0)\kappa + q(1)(\kappa-1) + q(2)\kappa + \ldots]\,\Delta\epsilon \tag{47}$$

$$- [q(0)(\kappa-1) + q(1)\kappa + q(2)(\kappa-1) + \ldots]\,\Delta\epsilon - 2c\epsilon, \tag{48}$$

$$= [q(0) - q(1) + q(2) + \ldots]\,\Delta\epsilon - 2c\epsilon, \tag{49}$$

$$= |Q(z)|_{BAF}\Delta\epsilon - 2c\epsilon, \tag{50}$$

where $|Q(z)|_{BAF}$ is the "back-and-forth" impulse response sum of discrete control law $Q(z)$,

$$|Q(z)|_{BAF} = \sum_{k=0}^{p-1} (\text{-}1)^k q(k). \tag{51}$$

Therefore, we obtain a necessary condition for no *continuous* energy generation for arbitrary (malicious) human movement,

$$c > |Q(z)|_{BAF}\frac{\Delta}{2}. \tag{52}$$

Inequality (52) matches the results of Abbott and Okamura [1] and Diolaiti et al. [8], which established that for a virtual spring rendering with stiffness K, limit cycles could occur if the energy leaks from quantization were not be entirely dissipated by Coulomb friction, $K\frac{\Delta}{2} > c$.

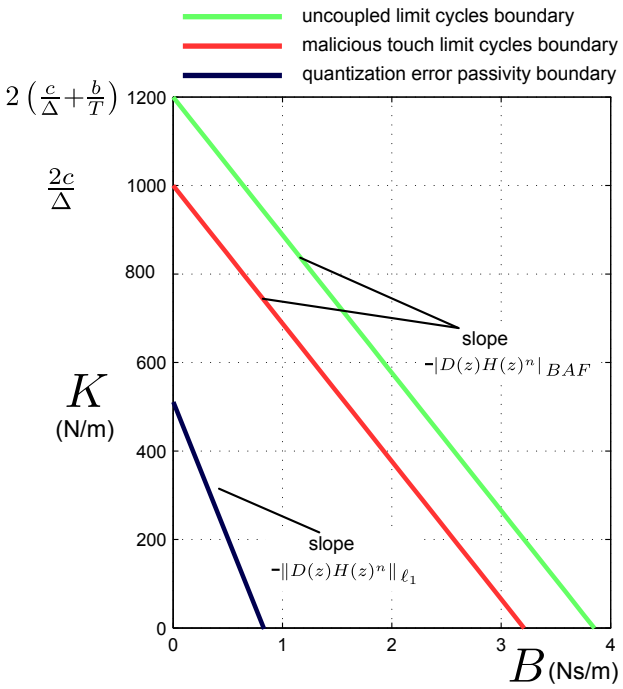

Fig. 18. Quantization error region boundaries. The regions are *under* the curves. The quantization error noise-free regions are expanded for a smaller quantization interval, larger Coulomb friction, and more aggressive low-pass filtering.

3) Necessity for no uncoupled continuous energy generation "uncoupled vibrations": Inequality (45) is a necessary condition for no continuous energy generation for *arbitrary* (malicious) trajectories. Here we present a condition for *uncoupled* (no human interaction) quantization error limit cycles. We consider a relatively likely limit cycle trajectory spanning a single quantization interval compared to the "back-and-forth" trajectory that straddles a quantization interval an infinitesimally small distance. Because the uncoupled limit cycle spans a quantization interval, the energy dissipation due to viscous damping is not negligible compared to the dissipation due to Coulomb friction. Thus, a necessary condition for no continuous energy generation is

$$c+\frac{b\Delta}{T} > |Q(z)|_{BAF}\frac{\Delta}{2}. \tag{53}$$

In other words, if Inequality (53) is not satisfied, the uncoupled haptic display can continuously create energy due to quantization error.

Figure 18 shows the quantization error region boundaries for $\Delta = 0.0002$ m, $T = 0.001$ s, $c = 0.1$ N, $b = 0.1$ Ns/m, $f_0 = 50$ Hz, and $n = 1$. Larger Coulomb friction, smaller quantization intervals, and more aggresive filtering expands the quantization error noise-free regions. The largest quantization error noise-free virtual stiffness is achieved for no virtual damping. Table III summarizes the quantization error region conditions.

TABLE III

QUANTIZATION ERROR CONDITIONS

Quantization error passive	
Sufficiency over	$c > \|\|Q(z)\|\|_{\ell_1}\Delta$
any time and any trajectory	
No malicious touch vibrations	
Necessity over	$c > \|Q(z)\|_{BAF}\frac{\Delta}{2}$
all time and any trajectory	
No uncoupled vibrations	
Necessity over	$c + \frac{b\Delta}{T} > \|Q(z)\|_{BAF}\frac{\Delta}{2}$
all time and uncoupled	

Fig. 19. The experimental setup. Experiments were performed on a single joint of the Phantom Premium 1.5. All other joints were mechanically constrained by a mechanical fixture displayed in the circle.

VI. EXPERIMENTS

In this section we present the results of experiments conducted to compare to theoretical predictions. The experiments were conducted on a single joint of the Phantom Premium 1.5 haptic device (the first revolute joint) while the other degrees of freedom were mechanically constrained by a fixture (Figure 19). A time-based system identification procedure was performed to find the mass, viscous damping, and Coulomb friction of the open-loop device [6]. The means and standard deviations of the estimates for the haptic device parameters over ten trials are shown in Table IV.

TABLE IV

HAPTIC DEVICE FIT PARAMETERS

Obj. Func.	$\hat{m}$ (g)		$\hat{b}$ (Ns/m)		$\hat{c}$ (N)	
	mean	σ	mean	σ	mean	σ
ℓ_2	94	4	0.10	0.02	0.11	0.04
ℓ_1	88	3	0.14	0.02	0.08	0.04

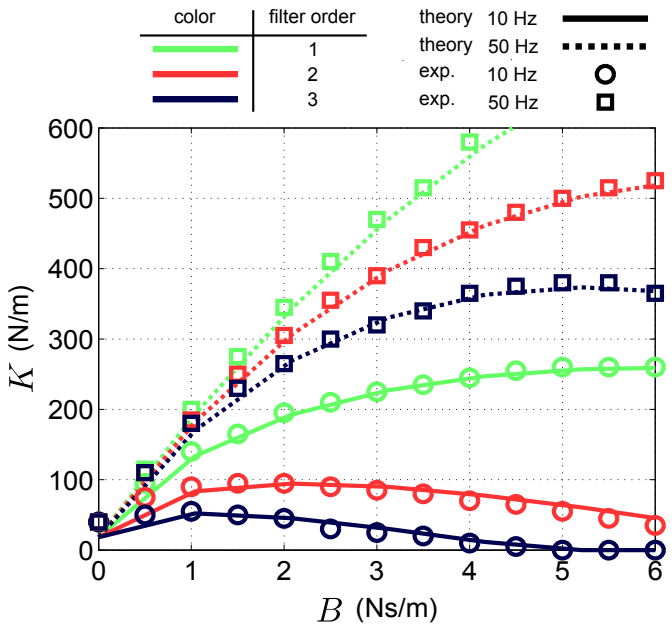

Fig. 20. Experimental and theoretical stability boundaries of the Phantom Premium 1.5 with $T = 0.001$ s, $t_d = 0.005$ s, for various cut-off frequencies and filter orders. The experimental data are similar to theoretical preditions.

A. *Uncoupled Stability Experiments*

Experimental stability boundaries were formed for the uncoupled (no human interaction) haptic display. For an experiment, the virtual stiffness was increased from zero in small increments and the system responses to strong impulses were measured. Instability was detected at the virtual stiffness value where growing oscillations were detected. Theoretical stability boundaries were found using the general stability condition (Inequality 21), and the device model of the ℓ_2 objective function of Table IV: $m = 94$ g, $b = 0.1$ Ns/m, and $c = 0.11$ N.

Figure 20 shows the experimental and theoretical stability boundaries for $T = 0.001$ s, $t_d = 0.005$ s, and various cut-off frequencies and filter orders.

The time delay was implemented in software in multiples of the sample time. These parameters were chosen to encounter stability boundaries at lower levels of virtual stiffness than quantization error

boundaries. The uncoupled experimental data were very consistent: for a certain experiment condition, the experimental virtual stiffness values for instability varied by less than 10 N/m. For this reason, we do not show the standard deviations of the experimental data in Figure 20.

B. Quantization Error Experiments

Quantization error experiments were conducted to compare to theoretical predictions. We manipulated the position quantization of the system in software, and tested two types of quantization error limit cycles: uncoupled vibrations and malicious touch vibrations. For both sets of experiments the magnitude of the virtual stiffness was increased in small intervals starting from zero, and the system response was measured. A quantization error boundary was detected when sustained (bounded) oscillations were detected.

For the uncoupled vibration experiments, there was no external interaction with the haptic display. The system was excited with a strong impulse force.

For the malicious touch vibration experiments, a user employed a strategy to elicit quantization error energy [1]. This was done by the user pressing lightly on the haptic manipulandum near a quantization boundary. If sustained vibrations occurred, the display would oscillate very quickly at a frequency near ω^* given by Equation (27). In these experiments, the user was attempting to touch the wall with a constant force; the oscillations seen were not the result of volitional movement.

Figure 21 shows the experimental data and the theoretical quantization error boundaries for a low-pass cut-off frequency of $f_0 = 30$ Hz, a filter order of $n = 1$, and an artificial quantization interval of $\Delta = 0.0015$ m. The natural quantization of the Phantom Premium is $\Delta = 52.5$ μm.

The quantization error experimental data were not as consistent as the uncoupled stability data. For this reason, we show the mean and standard deviation for each test condition.

VII. Conclusion and Future Work

The main results of our research were the presentation of explicit stability and quantization error regions for virtual spring and damper rendering. Using these results, aided by the software included in the Appendix, system parameters to satisfy desired haptic display objectives (e.g., uncoupled stability, or quantization error passivity), can be chosen to create high-quality rendering of stiff dyanamics. Because trade-offs exist between stability, quantization error noise rejection, and accuracy (e.g., more aggressive low-pass filtering results in less quantization error, but also reduces stability and accuracy), there is no single optimal system design. We verified our analytical results with experimental data using a Phantom Premium 1.5 haptic device.

Most current-day impedance-type, kinesthetic, haptic devices are designed with as little mass, damping, and friction as possible to reduce free-space motion forces with no feedback. With this design methodology,

(a)

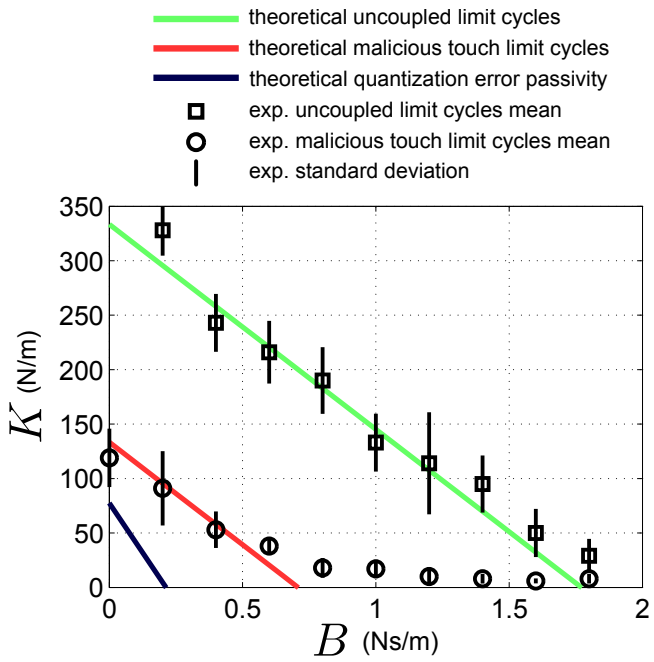

(b)

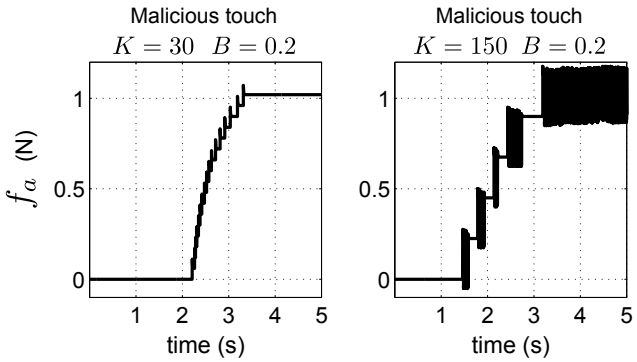

(c)

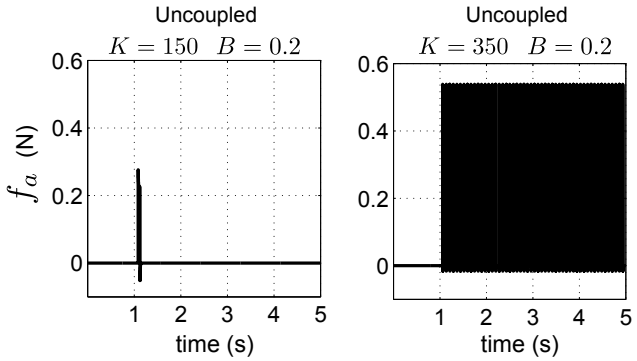

Fig. 21. (a) Experimental quantization error data for malicious touch and uncoupled limit cycles, and theoretical quantization error boundaries. (b) Malicious touch actuator force time histories with $B = 0.2$ Ns/m for no limit cycles at $K = 30$ N/m (left), and limit cycles at $K = 150$ N/m (right). (c) Uncoupled actuator force time histories with $B = 0.2$ Ns/m for no limit cycles at $K = 150$ N/m (left), and limit cycles at $K = 350$ N/m (right).

the minimum haptic display impedance is the open-loop (no haptic feedback) dynamics of the haptic device, and the maximum impedance is rendered using haptic feedback, usually by rendering a virtual spring damper. Our results show that the maximum impedance is increased for larger device damping (to make the system more stable), and larger friction (to make the system less sensitive to quantization error). However, increasing damping and friction also increases the minimum haptic display impedance. This presents a trade-off between rendering small forces in free-space motion and rendering large forces for stiff dynamics. An area for future work is to examine intentionally increasing device damping and friction to expand the upper impedance range, and using haptic feedback to *compensate* the unwanted free-space forces that this would introduce.

We chose a very basic low-pass filter type to simplify the analysis. The qualitative results for sampled data passivity, uncoupled stability, quantization error, and accuracy extend to other filter types, where the cut-off frequency and filter order correspond to the bandwidth and roll-off of the frequency response of other low-pass filter types, respectively, presented here. The general sampled data passivity condition, Inequality (13), stability condition, Inequality (21), and quantization error energy conditions, Inequalities (45), (52), and (53) are applicable to any low-pass filter type.

Many models could be used to describe a haptic display rendering a virtual spring and damper; our choice of models shown in Figure 2 were driven by relevance as a practical design tool, tractability for finding solutions, and our ideas about the most significant factors in system stability and quantization error. In future work, we could capture additional system properties, such as haptic device coupling vibrational modes, and multiple degrees of freedom.

Appendix A: Index to Multimedia Extensions

Archives of IJRR multimedia extensions published prior to 2014 can be found at http://www.ijrr.org. After 2014 all videos are available on the IJRR YouTube channel at http://www.youtube.com/user/ijrrmultimedia

Table of Multimedia Extensions

Extension	Type	Description
1	Code	`ComputeSpringDamperRendering StabilityAndQuantizationErrorLimits.m` Matlab function that takes in haptic display parameters and outputs stability and quantization error limits for virtual spring damper rendering.
2	Code	`SpringDamperRenderingExample.m` Matlab example code that shows how Extension 1 can be used for typical applications.

ACKNOWLEDGMENT

This work was supported in part by National Science Foundation grant 1217635.

REFERENCES

[1] J. J. Abbott and A. M. Okamura. Effects of position quantization and sampling rate on virtual-wall passivity. *IEEE Transactions on Robotics*, 21(5):952–964, 2005.

[2] V. Chawda, O. Celik, and M. K. O'Malley. A method for selecting velocity filter cutoff frequency for maximizing impedance width performance in haptic interfaces. *Journal of Dynamic Systems, Measurement, and Control*, 137(2), 2014.

[3] J. E. Colgate. Strictly positive real admittances for coupled stability. *Journal of the Franklin Institute*, 329(3):429–444, 1992.

[4] J. E. Colgate and J. M. Brown. Factors affecting the z-width of a haptic display. In *Proc. IEEE International Conference on Robotics and Automation*, pages 3205–3210, 1994.

[5] J. E. Colgate and G. G. Schenkel. Passivity of a class of sampled-data systems: Application to haptic interfaces. *Journal of Robotic Systems*, 14(1):37–47, 1997.

[6] N. Colonnese, S. M. Sketch, and A. M. Okamura. Closed-loop stiffness and damping accuracy of impedance-type haptic displays. In *Haptics Symposium*, pages 97–102, Feb 2014.

[7] I. Diaz and J. J. Gil. Influence of vibration modes and human operator on the stability of haptic rendering. *IEEE Transactions on Robotics*, 26(1):160–165, Feb 2010.

[8] N. Diolaiti, G. Niemeyer, F. Barbagli, and J. K. Salisbury. Stability of haptic rendering: Discretization, quantization, time delay, and coulomb effects. *IEEE Transactions on Robotics*, 22(2):256–268, 2006.

[9] G. F. Franklin, M. L. Workman, and D. Powell. *Digital Control of Dynamic Systems*. Addison-Wesley Longman Publishing Co., Inc., Boston, MA, USA, 3rd edition, 1997.

[10] G. F. Franklin, D. J. Powell, and A. Emami-Naeini. *Feedback Control of Dynamic Systems*. Prentice Hall PTR, Upper Saddle River, NJ, USA, 4th edition, 2001.

[11] J. Gil, T. Hulin, C. Preusche, E. Sánchez, and G. Hirzinger. Stability boundary for haptic rendering: Influence of damping and delay. *Journal of Computing and Information Science in Engineering*, 9(1):1–8, 2009.

[12] P. G. Griffiths, R. B. Gillespie, and J. S. Freudenberg. A fundamental tradeoff between performance and sensitivity within haptic rendering. *IEEE Transactions on Robotics*, 24(3):537–548, 2008.

[13] P. G. Griffiths, R. B. Gillespie, and J. S. Freudenberg. A fundamental linear systems conflict between performance and passivity in haptic rendering. *IEEE Transactions on Robotics*, 27(1):75–88, 2011.

[14] T. Hulin, C. Preusche, and G. Hirzinger. Stability boundary for haptic rendering: Influence of human operator. In *IEEE International Conference on Intelligent Robots and Systems*, pages 3483–3488, 2008.

[15] H. K. Khalil. *Nonlinear Systems*. Prentice Hall, 3 edition, 2001.

[16] J. E. Slotine and W. Li. *Applied nonlinear control*. Pearson, Upper Saddle River, NJ, 1991.

[17] K. Zhou, J. C. Doyle, and K. Glover. *Robust and Optimal Control*. Prentice-Hall, Upper Saddle River, NJ, 1996.